Journal of Hazardous Materials 198 (2011) 78–86

Contents lists available at SciVerse ScienceDirect

Journal of Hazardous Materials

journal homepage: www.elsevier.com/locate/jhazmat

High photoactive and visible-light responsive graphene/titanate nanotubes photocatalysts: Preparation and characterization

Zhai Qianqian, Bo Tang, Hu Guoxin*

School of Mechanical and Power Engineering, Shanghai Jiaotong University, No.800 Dongchuan Road, Shanghai 200240, China

ARTICLE INFO

Article history:
Received 4 July 2011
Received in revised form
26 September 2011
Accepted 3 October 2011
Available online 6 October 2011

Keywords:
Photocatalysts
Graphene
Titanate nanotubes
Sensitization

ABSTRACT

A series of graphene/titanate nanotubes (TNTs) photocatalysts using graphene and nanoscale TiO_2 or P25 as original materials were fabricated by hydrothermal method. Both low hydrothermal temperature and proper amount of graphene are propitious to better photoactivity. The photocatalytic activities of these nanocomposites far exceed that of P25, pure TNTs and reported TiO_2-based nanocomposites for the degradation of Rhodamine-B under visible-light irradiation. These prepared photocatalysts were characterized by TEM, XRD, XPS, BET, FTIR and UV–vis diffuse reflection spectra, and the results indicate that the outstanding photoactivities in visible-light region result from sensitization effect of graphene rather than impurity level in the band gap of TNTs. Furthermore, large BET surface areas of these photocatalysts (almost 10 times larger than that of previously reported graphene/TiO_2 nanoparticles) evidently enhance their absorption abilities and photocatalytic performances (the rate constants of degrading Rhodamine-B are at least 5 times higher than that of previously reported photocatalysts). These photocatalysts show good stability, and their photoactivities do not obviously decrease after four times of repeated uses. A detailed photocatalytic mechanism is suggested, as well.

1. Introduction

Graphene, a semi-metal material with zero band gap, has attracted intense attention since it was discovered by Geim et al. in 2004 [1]. The novel two-dimensional material possesses excellent electrical and optical properties, large specific surface area and outstanding mechanical property [2,3]. Recently, Peak et al. proved that graphene nanosheets can play as electronic conductive channels to improve the electrochemical performance of the graphene–SnO_2 composite [4]. Seger and Kamat demonstrated that graphene is an effective support material to disperse Pt nanoparticles [5]. Therefore, graphene is expected to serve as a scaffold to anchor nanoscale semiconductor photocatalyst and as a photosensitizer to enhance their photocatalytic activity under visible-light illumination at the same time.

TiO_2 and titanate nanotubes (TNTs) have been widely studied in some fields including photolysis of organic pollutant, hydrogen production and dye-sensitized solar cell [6–9]. In recent years, increasing interests have been focused on constructing visible-light driven TiO_2 owing to its obvious advantage on utilization of solar energy. One method is metal/nonmetal doping, which introduces an impurity level in the band gap and increases visible-light absorbance [10–17]. However, the foreign dopant may act as a combination center for photogenerated electron-hole pairs [10–12]. Another approach to extend the optical response of TiO_2 into visible-light region is coating, such as noble metal coating, dye coating [18,19]. Carbonaceous material coated TiO_2 has always attracted much attention for its excellent photocatalytic activity. Recently, due to unique merits of graphene, modifying TiO_2 with graphene has attracted a great deal of attention. Zhang et al. synthesized graphene–TiO_2 nanocomposite to derive hydrogen by splitting water [20]. Compared to that of P25, the amount of hydrogen evolution is 1.9 times larger by using this photocatalyst. Zhang et al. prepared P25–graphene nanocomposite to degrade methylene blue [21]. The photocatalytic performances demonstrated that graphene could obviously enhance photocatalytic activity of P25 under both visible and UV light illumination.

Numerous researches on extending the optical response of TiO_2 to visible-light have been made. However, similar reports on TNTs were rare. In fact, the unique physical properties of TNTs, including open mesoporous morphology and high BET surface area, are benefit to adsorbability as well as photocatalytic performance. However, to the best of our knowledge, no paper on graphene hybridized TNTs has been reported. Herein, we synthesized a series of graphene/TNTs nanocomposites with hydrothermal method by using graphene and nanoscale TiO_2 or P25 as original materials. These prepared photocatalysts possess large BET surface areas and outstanding photocatalytic activities to decompose

* Corresponding author. Tel.: +86 21 34206569; fax: +86 21 34206569.
E-mail address: hugx@sjtu.edu.cn (H. Guoxin).

0304-3894/$ – see front matter © 2011 Elsevier B.V. All rights reserved.
doi:10.1016/j.jhazmat.2011.10.012

Rhodamine-B (RB) under visible-light illumination. Moreover, no obvious decreases in the photoactivities were observed for the recycled photocatalysts. The BET surface areas of prepared photocatalysts are almost 10 times larger than that of previously reported graphene–TiO_2 photocatalyst [20]. After breaking the TNTs by sintering the as-prepared samples at high temperature, the BET surface areas and photocatalytic activities decreased significantly, indicating the importance of BET surface area. The influences from the graphene content and hydrothermal temperature are also discussed. Furthermore, a detailed photocatalytic mechanism is suggested, as well.

2. Experimental

2.1. Materials and chemicals

Nanoscale TiO_2 was purchased from Shanghai Jianghu industrial Co., Ltd. P25 (20% rutile phase and 80% anatase phase) was purchased from Degussa. Natural graphite power was obtained by Alfa Aesar Co. RB and sodium dodecyl sulfate (SDS) were obtained commercially from the Beijing Chemical Reagent Plant. Deionized water (resistivity 18 MΩ cm) was utilized to prepare all aqueous solution and to rinse the specimens.

2.2. Preparation of photocatalysts

These photocatalysts are denoted as 120 °C G/T, 150 °C G/T, 180 °C G/T (graphene and nanoscale TiO_2 as starting materials at 120 °C, 150 °C and 180 °C hydrothermal treatment, respectively) and 120 °C G/P, 150 °C G/P, 180 °C G/P (graphene and P25 as starting materials at 120 °C, 150 °C and 180 °C hydrothermal treatment, respectively). Moreover, G/T-X and G/P-X represent samples containing X wt% (X = 1, 5, 10) graphene.

Firstly, modified Hummers' method was used to prepare graphene oxide (GO) [22,23] and then hydrazine was adopted to achieve the reduction of GO to graphene in 98 °C water bath for 2 h. In a typical procedure for preparing 120 °C G/T-5 and 120 °C G/P-5, 50 mg graphene was added to 2 mL (1 mol/L) SDS solution. Subsequently, 38 mL deionized water was added and then the mixture was treated with ultrasonic for 1 h. The SDS was used to stabilize the graphene in aqueous solution [24]. After ultrasonic processing, 1 g nanoscale TiO_2 (or P25) was added to the solution under modest stirring. Then 40 mL (20 mol/L) NaOH aqueous solution was added under stirring. At last, the mixture was transferred to an autoclave, followed by hydrothermal reaction at 120 °C for 18 h. Similarly, 10 mg and 100 mg of graphene were used to prepare the G/T(P)-1 and G/T(P)-10, respectively. After hydrothermal reaction, the product was purified (centrifugation, washing with water and re-dispersion for 4 cycles, washing with 0.1 mol/L HCl, washing with water until the washing solution achieved pH 7) and then grinded to powder after dried in oven at 80 °C for 5 h. The pure TNTs were prepared by similar process without adding graphene.

2.3. Characterization and photocatalyst measurements

The TEM images were carried out using JEM-2100F at 200 kV. The BET surface areas were measured on a Nova 100 by using N_2 as the adsorption gas. UV–vis diffuse reflectance spectra were recorded on a TU-1901 UV–vis spectrophotometer. X-ray diffraction (XRD) patterns were recorded on Bruker D8 Advance (Cu Kα radiation 0.154 nm). Fourier transform infrared spectroscopy (FTIR) curves were measured on IR Prestige-21 system (PerkinElmer). X-ray photoelectron spectroscopy (XPS) measurements were performed on a RBD upgraded PHI-5000C ESCA system (Perkin Elmer). Electron paramagnetic resonance (EPR) results were recorded on EPR-8 (Bruker BioSpin Corp., Germany).

The photocatalytic reaction system consists of a 500 W xenon lamp and a cutoff filter (1 mol/L $NaNO_2$ solution in an enclosed vessel (λ > 400 nm) or another cutoff filter (λ > 610 nm)). Visible-light photocatalytic activities of all photocatalysts were evaluated by degradation of RB. In a typical process, 15 mg photocatalyst was dispersed into 50 mL RB solution (10 mg/L). The suspension was treated with ultrasonic for 10 min and stirred for another 60 min in dark to reach an adsorption balance. The resulting suspension was irradiated under visible-light, and the concentration of RB solution was monitored by UV-721 spectrometer at 553 nm at regular time intervals. Typically, 2 mL solution was taken and centrifuged (4000 rpm for 10 min). After removing the sediment (photocatalyst particles), the supernatant was used to analyze.

3. Results and discussion

3.1. Decomposition of RB

The concentration changes of RB in the presence of different photocatalyst as a function of visible-light irradiation time are shown in Fig. 1. Therein, the C_0 represents the remaining concentration of RB after the adsorption equilibrium before light illumination, while C_t represents the remaining concentration of RB after light illumination with a specific time. As shown in Fig. 1a, attributed to their wide band gaps, both P25 and pure TNTs can hardly decompose RB under visible-light irradiation for 40 min. We found that 65% and 61% RB were degraded by using P25 and pure TNTs when the irradiated time of visible-light is extended to 4 h, respectively (see Fig. S1a of Supplementary material). Therefore, the result demonstrates that the self-photolysis effect (dye sensitization) of RB is not obvious in a short time (40 min). However, more than 70% RB were degraded by using any G/T or G/P after 40 min visible-light irradiation, and the rate constants are at least 5-fold faster than that of previously reported TiO_2-based photocatalysts (the rate constants are shown in Table 1) [16,25–27]. In order to rule out the self-photolysis of RB, we have adopted another cutoff filter (λ > 610 nm) to do the degrading experiment (the maximum absorption wavelength of RB is around 553 nm). We found that RB could not be degraded by using pure TNTs under visible-light illumination for 7 h, while about 80% RB was degraded by using G/T (G/P) under the same conditions (see Fig. S1b of Supplementary material). Therefore, the visible-light responses of G/T and G/P result from the sensitization of graphene, which will be further discussed in Sections 3.2, 3.4 and 3.6. Based on detailed observation of Fig. 1a–c, both G/T-5 and G/P-5 possess best photocatalytic activities, and more than 90% RB were degraded within 40 min visible-light irradiation (except 88% and 86% for 180 °C G/T-5 and 180 °C G/P-5, respectively). As for G/T(P)-1 and G/T(P)-10, about 55 and 65 min are needed to degrade 90% RB under visible-light illumination, respectively. The inset of Fig. 1a clearly demonstrates that the photocatalytic performances of 120 °C G/T(P)-5 are better than that of 120 °C G/T(P)-1 and 120 °C G/T(P)-10 (the 150 °C and 180 °C samples demonstrate similar results). The reason can be explained as follows: insufficient graphene (1 wt%) could not provide enough photogenerated electrons and electron transportation channels to TNTs, while excessive graphene would shield the light reaching the surface of the TNTs (increased absorbance and scattering of photons by phonons of graphene). Therefore, the results indicate the synergetic effect of graphene and TNTs.

Moreover, the photocatalytic performances of these photocatalysts decrease in the order 120 °C samples > 150 °C samples > 180 °C samples, indicating that the photoactivity is related to the hydrothermal temperature (the lower hydrothermal temperature is good for better photoactivity). It is necessary to consider the stabilities of these photocatalysts in the practical water purification

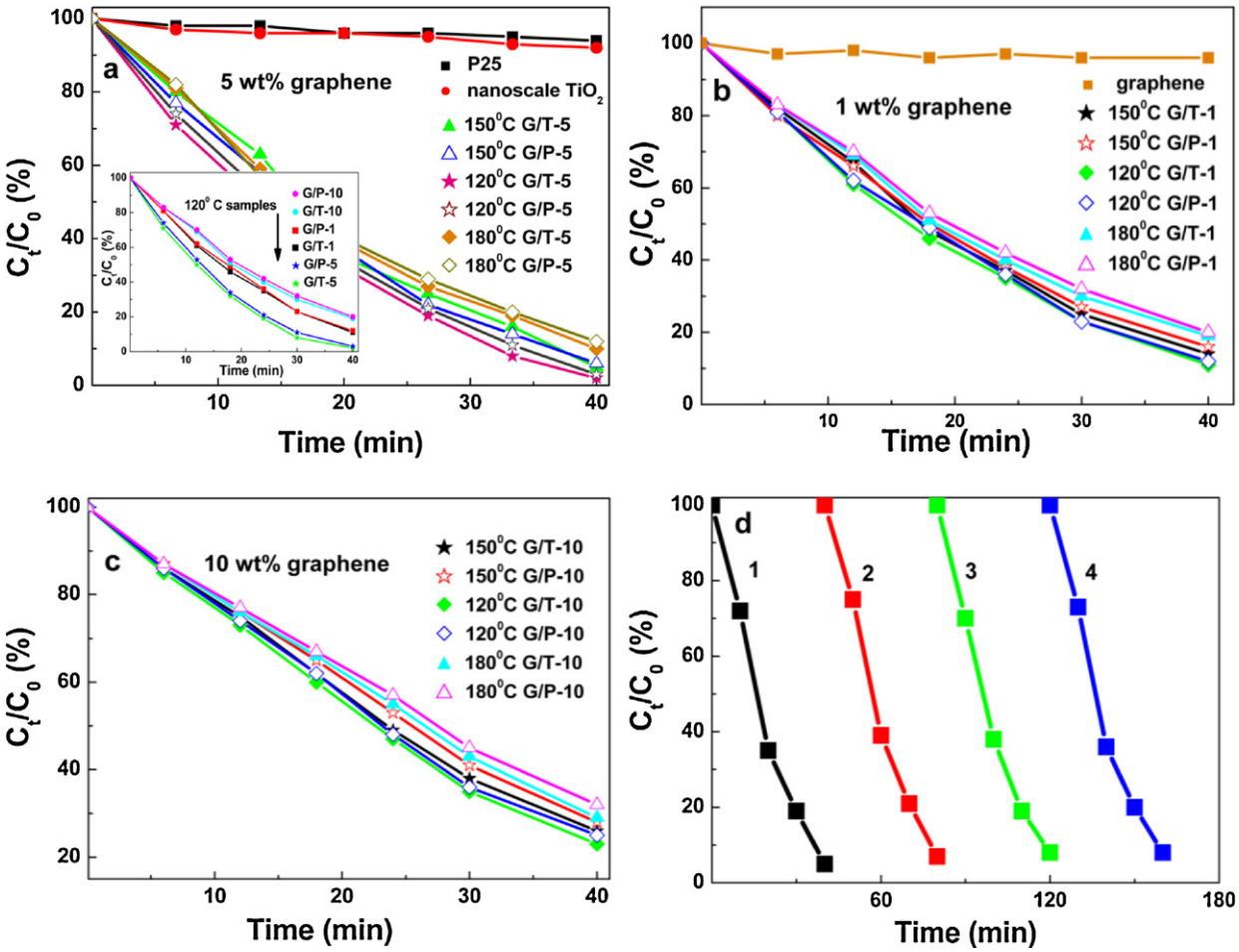

Fig. 1. Degradation of Rhodamine-B under visible-light illumination with (a) P25, nanoscale TiO_2, G/T-5 and G/P-5 prepared at varied temperatures, and the inset shows the influence on photocatalytic performances from graphene contents, (b) pure graphene, G/T-1 and G/P-1 prepared at varied temperatures, (c) G/T-10 and G/P-10 prepared at varied temperatures, (d) photoactivity stability test of 150 °C G/T-5; 1–4 represent first to fourth cycle, respectively.

Table 1
Rate constants of P25, nanoscale TiO_2, as-prepared photocatalysts and previously reported TiO_2-based photocatalysts on degrading Rhodamine-B under visible-light illumination ($\lambda > 400$ nm) are shown.

Photocatalysts	Reaction time (min)	RB degradation efficiency (%)	Rate constant (min^{-1})
P25	40	8	$<2.03 \times 10^{-3}$
Nanoscale TiO_2	40	6	$<1.54 \times 10^{-3}$
Pure TNTs	40	10	$<2.63 \times 10^{-3}$
120 °C G/T-1	40	89	5.52×10^{-2}
120 °C G/P-1	40	88	5.30×10^{-2}
120 °C G/T-5	40	97	8.76×10^{-2}
120 °C G/P-5	40	96	8.05×10^{-2}
120 °C G/T-10	40	80	4.02×10^{-2}
120 °C G/P-10	40	77	3.67×10^{-2}
150 °C G/T-1	40	86	4.92×10^{-2}
150 °C G/P-1	40	84	4.58×10^{-2}
150 °C G/T-5	40	90	5.76×10^{-2}
150 °C G/P-5	40	93	6.65×10^{-2}
150 °C G/T-10	40	75	3.47×10^{-2}
150 °C G/P-10	40	72	3.18×10^{-2}
180 °C G/T-1	40	81	4.15×10^{-2}
180 °C G/P-1	40	74	3.38×10^{-2}
180 °C G/T-5	40	88	5.30×10^{-2}
180 °C G/P-5	40	86	4.92×10^{-2}
180 °C G/T-10	40	68	2.85×10^{-2}
180 °C G/P-10	40	71	3.09×10^{-2}
DBS–TiO_2 [25]	40	51	1.7×10^{-2}
Fe(0.5%)–TiO_2 [26]	240	20	$\sim 1 \times 10^{-3}$
Fe(0.1%)/Co(0.4%)–TiO_2 [26]	240	64	4.26×10^{-3}
Activated carbon–TiO_2 [27]	100	50	$(1 \pm 0.2) \times 10^{-2}$
H_2O_2–TiO_2(ultrasonic) [28]	120	80	1.5×10^{-2}

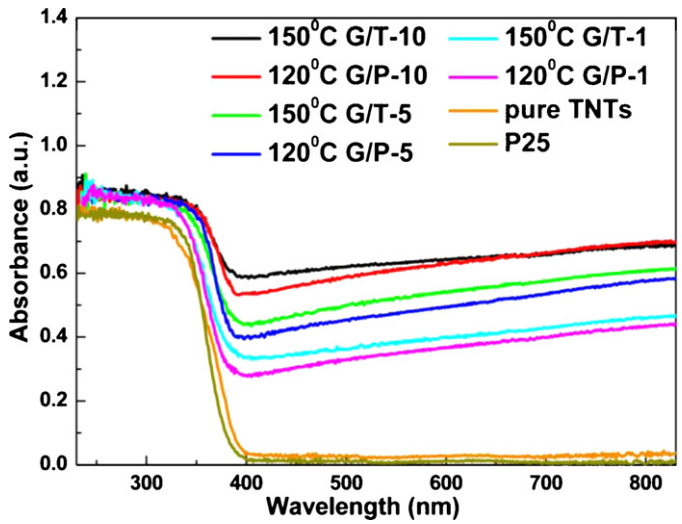

Fig. 2. UV–vis diffuse reflectance spectra of 150 °C G/T-10, 120 °C G/P-10, 150 °C G/T-5, 120 °C G/P-5, 150 °C G/T-1, 120 °C G/P-1, P25 and pure TNTs.

field. The stabilities of these samples were tested and the result of 150 °C G/T-5 is shown in Fig. 1d (the similar results of other photocatalysts were shown in Fig. S1c–e of Supplementary material). The results suggest that all the G/T and G/P are stable after 4 times repeated uses. The G/T-5 and G/P-5 were chosen for further analysis mainly because of their better photocatalytic performances.

3.2. Optical properties of photocatalysts

The optical properties of the 150 °C G/T-5 (1,10), 120 °C G/P-5 (1,10), P25 and pure TNTs are shown in Fig. 2. A significant increase in the absorption at the wavelength shorter than 400 nm can be seen for all the samples, which is assigned to the intrinsic band gap absorption of TiO_2 and TNTs. The results indicate that no carbon atom doped into the lattice of TNTs because impurity level would shift the absorption edge to the higher wavelength. On the other hand, compared with pure TNTs and P25, the presence of graphene obviously enhances visible-light absorption [20,28,29]. The increased absorbance in 400–850 nm with increasing amount of graphene (G/T(P)-10 > G/T(P)-5 > G/T(P)-1) is due to the colors becoming darker (see Fig. 8). Therefore, the high photocatalytic activities of these photocatalysts under visible-light illumination are attributed to the sensitization of graphene rather than impurity level in the band gap of TNTs.

3.3. XRD results

Fig. 3a shows the XRD patterns of 180° G/T-10, 150° G/T-5, 150° G/P-5, 120° G/P-1 and pure TNTs. It is obvious that the photocatalysts with different amounts of graphene exhibit similar XRD patterns. The diffraction peaks around 9°, 25°–28° and 47° can be assigned to tubular structure, (1 1 0), (0 0 3) and (0 2 0) crystal planes of TNTs, respectively [30,31]. Moreover, no typical diffraction peaks belonged to graphene can be found in these curves, which is in agreement with early reports [20,21,29,24]. The reason can be attributed to the disappearance of the layer-stacking regularity of graphene after reduction by hydrazine [32]. The XRD curves of nanoscale TiO_2, P25, the as-prepared 150 °C G/T-5, 350 °C and 600 °C sintered 150 °C G/T-5 are shown in Fig. 3b, respectively. Only pure anatase type (JCPDS card: 84-1286) can be found in nanoscale TiO_2, while both anatase and rutile phases (JCPDS card: 21-1276) can be seen in P25. The characteristic peaks of TNTs disappeared and were replaced by anatase TiO_2 peaks in sintered samples, meaning that the TNTs collapsed and transformed to anatase phase TiO_2 during the high temperature. Based on these results, it was found that: (1) similar structures of G/T and G/P indicate that the diversities of original materials (different crystal structures of nanoscale TiO_2 and P25) do not influence the reassembling process during the hydrothermal reaction; (2) the presence and amount of graphene do not affect the formation of TNTs during the hydrothermal reaction; (3) the temperatures of hydrothermal reaction do not obviously influence the structures of these photocatalysts.

3.4. FTIR measurement

The FTIR spectra of pure TNTs, pure graphene, all G/T-5 and G/P-5 are shown in Fig. 4. In these patterns, the low frequency absorption below 1000 cm^{-1} is assigned to the Ti–O–Ti vibration [33], while the broad absorption from 3000 to 3700 cm^{-1} is attributed to the O–H stretching vibration of the surface hydroxyl from adsorbed water [21]. The absorption around 1600 cm^{-1} of pure graphene and all prepared photocatalysts clearly shows the skeletal vibration of the graphene sheets, proving the effective hybridization of graphene in these photocatalysts [34]. Compared with that of pure TNTs (in order to compare these curves clearly, the pattern size of the pure TNTs was doubled), the absorption bands

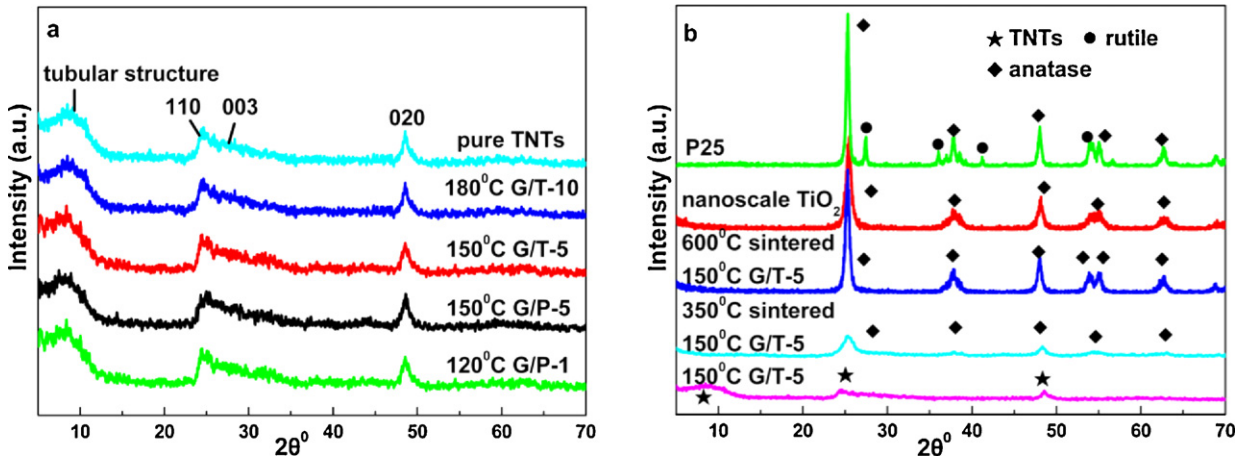

Fig. 3. XRD patterns of (a) pure TNTs, 180 °C G/T-10, 150 °C G/T-5, 150 °C G/P-5 and 120 °C G/P-1, (b) P25, nanoscale TiO_2, 600 °C sintered 150 °C G/T-5, 350 °C sintered 150 °C G/T-5 and as-prepared 150 °C G/T-5.

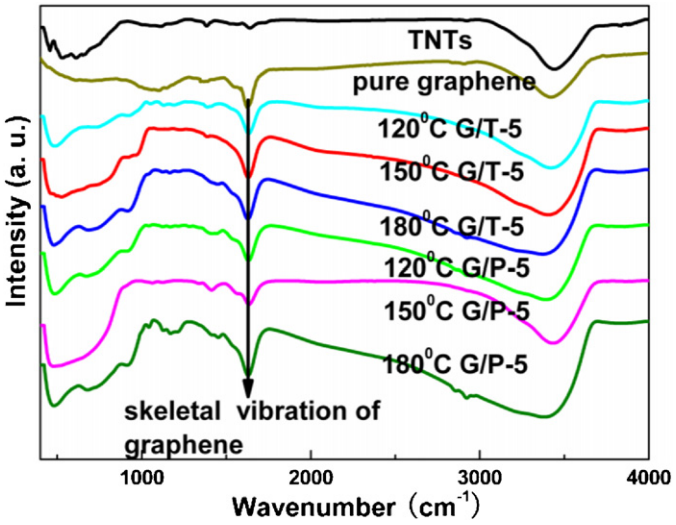

Fig. 4. FTIR curves of pure graphene, TNTs, 180 °C (150 °C, 120 °C) G/T-5 and G/P-5.

corresponding to Ti–O–Ti vibration (below 1000 cm^{-1}) become wider in all G/T-5 and G/P-5. In the previous report, this peak is suggested as a combination of Ti–O–Ti and Ti–O–C vibrations [35], indicating that the chemical bonds were built between graphene and TNTs through the residual surface hydroxyl groups of graphene [36,37]. No typical absorption bands belonging to Ti–C or C–O vibration can be found in these photocatalysts, suggesting no doped carbon existing in TNTs. The conclusion is in agreement with UV–vis diffuse reflectance spectra results.

3.5. TEM analysis

The TEM images of G/T-1, G/T-5, G/P-5, G/P-10 and 350 °C sintered G/T-5 (all photocatalysts were prepared with 150 °C hydrothermal reaction) are shown in Fig. 5a–e. The Fig. 5a–d shows representative TEM images of TNTs with different concentrations of graphene, and wrinkled graphene loaded on the TNTs surface (TNTs possess an average diameter of ~9 nm, samples prepared at 180 °C and 120 °C show similar results). Based on detailed analysis of the TEM images, the TNTs can be identified clearly in Fig. 5a because of the low content of graphene (1 wt%). On the contrary, the excess graphene (10 wt%) covered two sides of TNTs, so no TNTs were revealed obviously (Fig. 5d). Both TNTs and graphene can be seen in G/T-5 and G/P-5 from Fig. 5b and c (see inset of Fig. 5c), suggesting the proper proportion of graphene (5 wt%). From the above discussions, we can infer that G/T-5 and G/P-5 are more likely to exploit the merits of TNTs and graphene simultaneously, which is proved by degradation of RB. After 350 °C calcinations (G/T-5) for 2 h, TiO_2 nanoparticles instead of tubular TNTs can be seen in the Fig. 5e, which is in line with the XRD results. In some early reports, the TNTs keep tubular structure after high temperature process (400 °C). The different phenomenon in present work is due to the appearance of graphene. The different thermal expansivities between TNTs (positive value) and graphene (negative value) lead to a big stress in TNTs under high temperature. The stress broke the TNTs into nanoparticles and nanofragments during the sintering process. The typical high resolution TEM images of the G/T-5 and 350 °C sintered sample were shown in Fig. 5f and g. The TNTs with ~9 and ~7 nm in outer and inner diameters and several hundred nm in length are shown in Fig. 5f. The lattice fringes with 0.35 nm (layer spacing) showed in Fig. 5g are assigned to the (1 0 1) plane of the anatase TiO_2, which is proved by select area electron diffraction results (inset of Fig. 5g). The EDS results in Fig. 5h and i further confirm the effective hybridization of graphene in G/T and G/P (Fig. 5h and i represents G/T-1 and G/P-10, and the content of carbon obviously increased for G/P-10. The sign of copper is originated from copper grid). Moreover, the pure TNTs possess similar appearance as G/T-1 (see Fig. S2 in Supplementary materials), indicating that the additional graphene scarcely influences the formation of TNTs in hydrothermal reaction.

3.6. XPS results and photocatalytic mechanism

XPS was used to investigate the chemical states of C, O and Ti in the prepared photocatalysts. Fig. 6a–c shows the narrow scans of C, O and Ti of 120 °C G/T-5, 150 °C G/T-5 and 180 °C G/P-5, respectively. As shown in the XPS curves of C 1s (Fig. 6a), the strong single peak located at 284.7 eV is ascribed to the elemental carbon [28], while the weak shoulder peak centered at 288.9 eV is assigned to the absorbed CO_2 or residual hydroxyl functional groups of graphene [38]. The result is in excellent agreement with early reports on graphene–TiO_2 nanocomposites [20,39]. Further more, the absence of Ti–C bond around 281 eV again proved that the carbon atoms did not enter into the lattice of the TNTs. Fig. 6b shows O 1s narrow scan spectrum, and the peaks around 530.1 eV and 531.5 eV are attributed to the Ti–O and –OH adsorbed on the sample surface, respectively [40]. As for Ti 2p core level photoelectron spectrum, the peaks located at 458.7 eV and 464.5 eV are assigned to Ti 2p3/2 and Ti 2p1/2, respectively [41]. The results demonstrated that no Ti–C bonds are detected in these photocatalyst. The absence of peak around 457 eV implies that no Ti^{3+} ions are detected [42]. The existence of titanium only as Ti^{4+} ions means no doped carbon species in these photocatalysts. The doped carbon atoms always exist as substitutional carbon for oxygen or interstitial carbon, and the substitutional carbon would reduce the Ti–O bonds to yield the Ti^{3+} ions as well as the shift of Ti bond energy to lower value. Moreover, both substitutional and interstitial carbon species would yield C–O bonds and a new peak at 286–287 eV [39,43], which was denied by the results of C 1s curve. The XPS curves of 350 °C sintered 150 °C G/T-5 were shown in Fig. 6d. The profiles of O 1s and Ti 2p are similar with that of as-prepared photocatalysts (before calcinations), while some differences can be seen among the C 1s curves of them. The shoulder peak at 288.9 eV decreases significantly after calcinations, resulting from the removal of residual hydroxyl functional groups of graphene during the high temperature process.

Based on TEM, UV–vis diffuse reflectance spectra, FTIR and XPS results, we can infer that graphene loaded on the TNTs surface and carbon atoms did not dope into the lattice of TNTs. Therefore, the visible-light photoactivities of all prepared samples are due to the sensitization of graphene rather than impurity levels from doped carbon atoms. The photocatalytic mechanism of the G/T and G/P is suggested as follows: under visible-light irradiation, π state electrons were excited in the graphene by absorbing visible-light. Owing to the π–d conjugate, the π state electrons were subsequently injected into the conduction band of TNTs [29]. The high carrier mobility of graphene makes the photogenerated electrons transfer to TNTs quickly, which is in favor of utilizing efficiency of photogenerated electrons and high photoactivity. These electrons transferred to the surface of TNTs and reacted with oxygen to yield superoxide and hydroxyl radicals as follows [25,44]:

$$O_2 + e^-_{CB} \rightarrow O_2^- \quad (1)$$

$$2O_2^- + 2H^+ + e^-_{CB} \rightarrow OH^\bullet + OH^- + O_2 \quad (2)$$

The resulting radicals oxidize RB to yield CO_2, H_2O and other mineralization. The photocatalytic process was shown in Fig. 7. In order to further confirm this process, ESR analysis was used to detect the presence of O_2^- and $OH^\bullet$ radicals (5,5-dimethyl-1-pyrroline-*N*-oxide (DMPO) is a proper material to trap these radicals). As shown in Fig. 8a, four obvious peaks belonged to

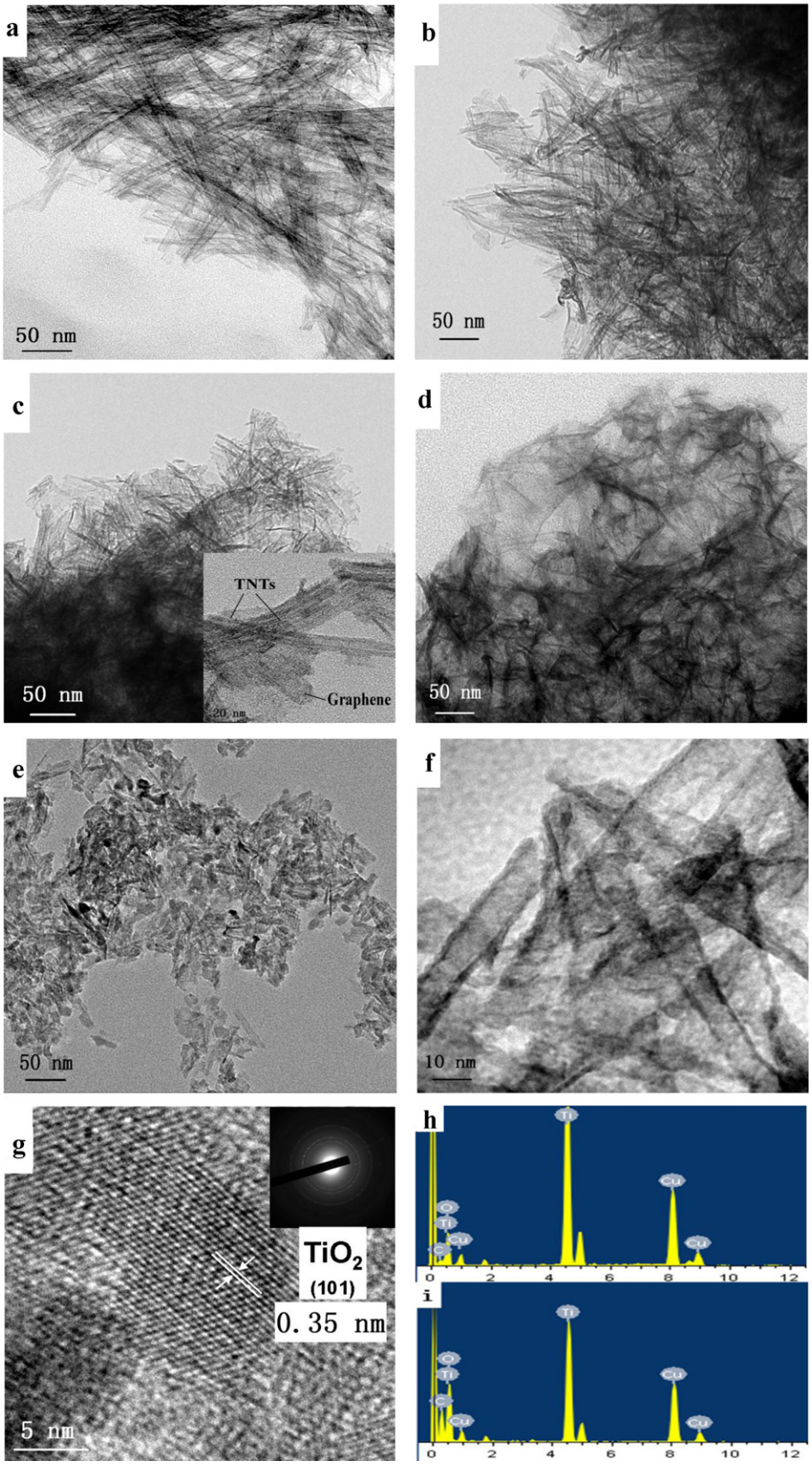

Fig. 5. TEM images of 150 °C hydrothermal reaction products. (a) G/T-1, (b) G/T-5, (c) G/P-5, graphene and TNTs can be seen and marked in the inset, (d) G/P-10, (e) 350 °C sintered G/T-5, (f) HRTEM image of G/T-5, (g) HRTEM image of 350 °C sintered G/T-5, (h and i) EDS of G/T-1 and G/P-10, respectively.

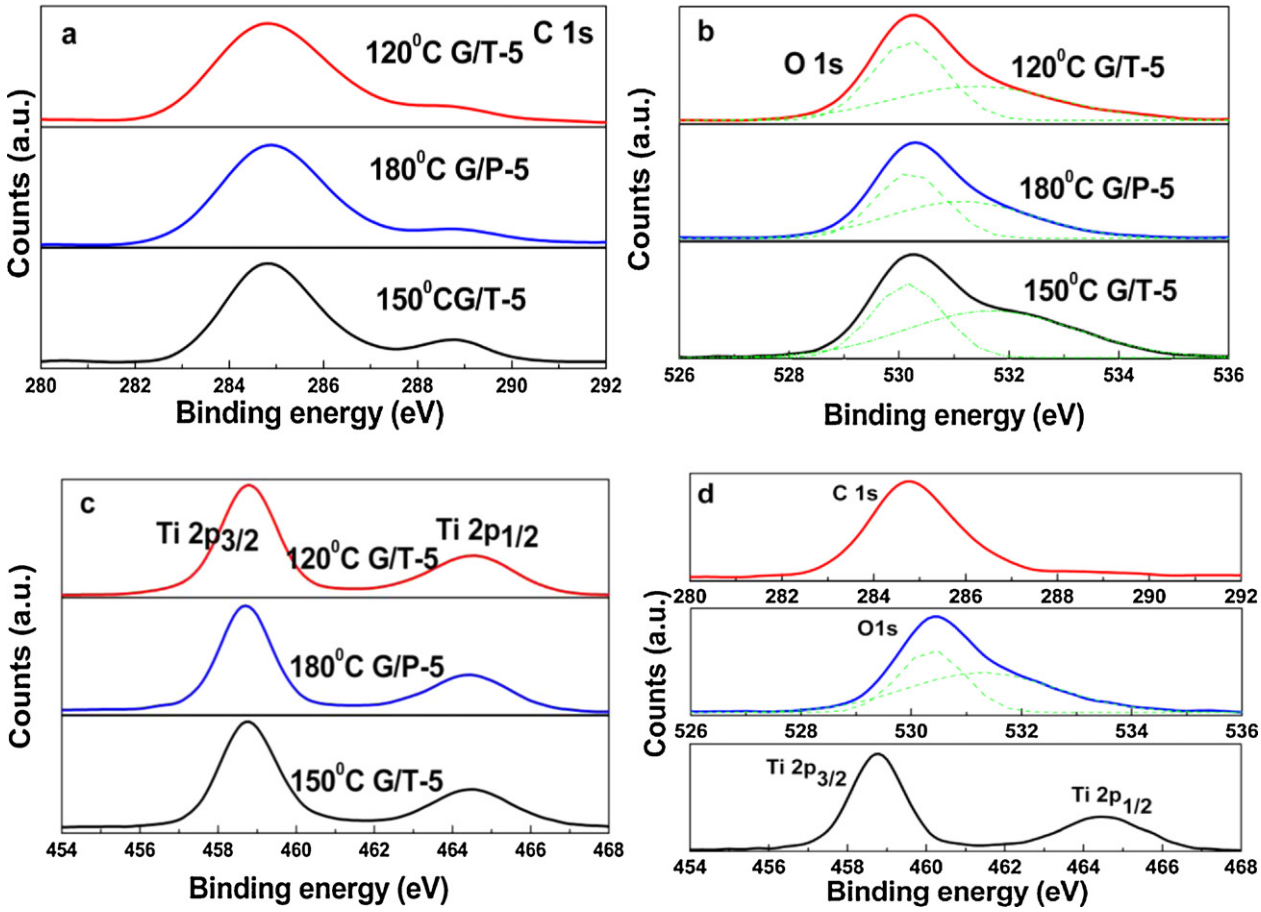

Fig. 6. XPS of the 120 °C G/T-5, 150 °C G/T-5 and 180 °C G/P-5. (a) C 1s, (b) O 1s, (c) Ti 2p, (d) 350 °C sintered G/T-5 (prepared with 150 °C hydrothermal reaction).

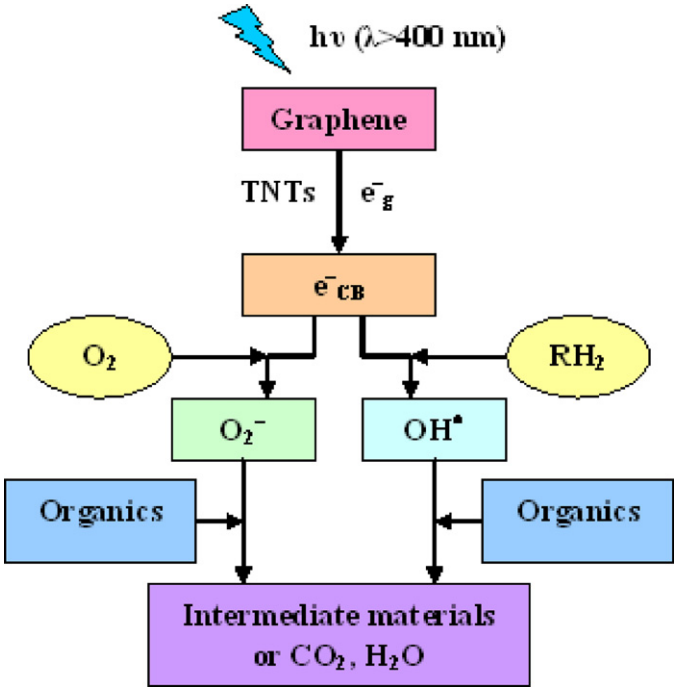

Fig. 7. Photocatalytic mechanism of all G/T and G/P, e_g^-, e_{CB}^- and RH_2 represent the photogenerated electrons of graphene, conduction band electrons of TNTs and reductant organic solute specifically absorbed on the photocatalysts surface, respectively.

DMPO–OH• can be seen by using 120 °C G/T-1 (5,10) under visible-light irradiation, while no peak can be detected by using pure TNTs. The similar results of DMPO–O_2^- were shown in Fig. 8b. Therefore, the visible-light responses of prepared photocatalysts originate from the added graphene. The intensities of both DMPO–OH• and DMPO–O_2^- peaks for G/T-5 are stronger than that of G/T-1 (10), indicating both the amounts of the produced OH• (O_2^-) radicals are highest by using G/T-5 (150 °C and 180 °C samples show similar results). The results are in great line with the degrading experiments. Moreover, separated graphene (without TNTs) does not degrade RB directly (see Fig. 1b), meaning that graphene is not a photocatalyst. Therefore, the graphene acts as sensitizer in these photocatalysts because the photogenerated electrons originated from it (the self-photolysis of RB can be ignored in our experiments which we have discussed in Section 3.1).

3.7. BET surface area

The BET surface areas of 120 °C G/T-5, 150 °C G/T-5 and 180 °C G/P-5 are almost 10 times larger than that of graphene–TiO_2 nanocomposite [20] and 6 times larger than graphene–P25 nanocomposite in previous reports (see Table 2) [21]. The large specific surface area is propitious to adsorption capacity as well as photocatalytic activity. Compared to P25 and nanoscale TiO_2, the adsorbabilities of G/T and G/P are greatly improved (Fig. 9). After 350 °C calcinations, the specific surface area of 150 °C G/T-5 decreased to 29 $m^2\,g^{-1}$, and the adsorbability and photocatalytic activity degrade obviously (Fig. 9 and Fig. 1S in Supplementary materials). Based on above results, we can see that (1) TNTs is a promising photocatalyst to hybridize with graphene because

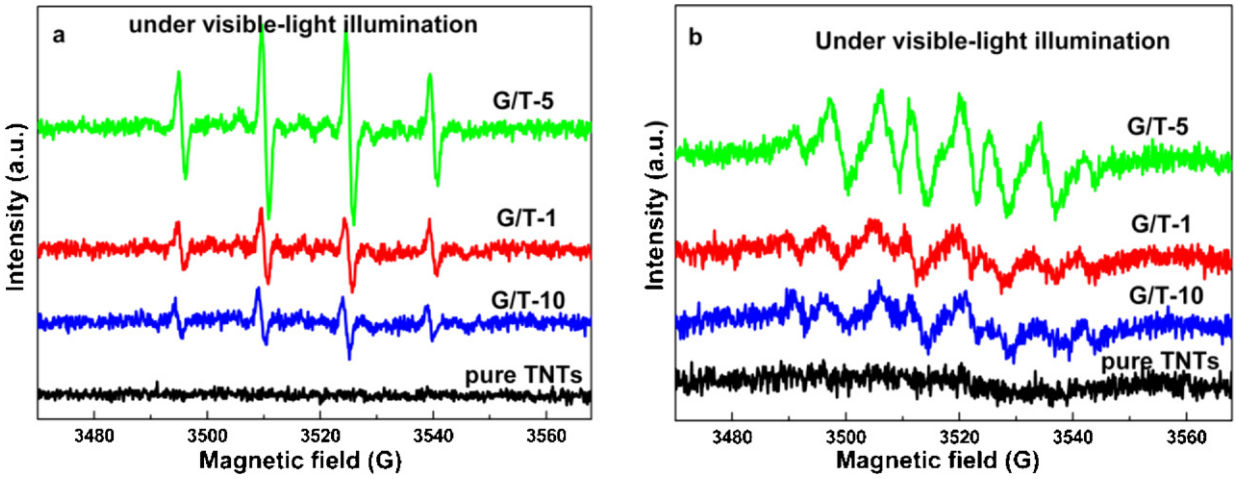

Fig. 8. EPR spectra of radical adducts trapped by DMPO in G/T-1 (5,10) and pure TNTs: (a) DMPO–OH• forming in visible-light irradiated aqueous dispersions; (b) DMPO–O_2^- forming in visible-light irradiated methanol dispersions.

Table 2
BET surface areas of pure TNTs, P25, nanoscale TiO_2, 120 °C G/T-5, 150 °C G/T-5, 180 °C G/P-5, 120 °C G/T-1, 120 °C G/T-10 and previously reported graphene–TiO_2 photocatalysts are demonstrated.

	TNTs/P25	Nanoscale TiO_2	120 °C G/T-5	150 °C G/T-5	180 °C G/P-5	120 °C G/T-1	120 °C G/T-10	350 °C sintered 150 °C G/T-5	TiO_2–GSs (1–10%)[20]	P25–GR/CNTs[21]
S_{BET} ($m^2\ g^{-1}$)	276.574/49.757	85.626	330.267	299.894	280.433	292.107	301.612	29.258	15.2–37.0	54.2/51.0

of its unique morphology and large BET surface area (larger than that of P25 and nanoscale TiO_2). (2) Low temperature hydrothermal method is in favor of bigger specific surface area to G/T and G/P. (3) Combining the results of Section 3.1, the distinctions of BET surface areas between these photocatalysts may be a partial reason for the differences of their photocatalytic performances. (4) Moreover, the removal of residual hydroxyl functional groups of graphene (350 °C sintered sample), which act as the bridges of graphene and TNTs, is another reason (except for the decreased BET surface area) for the severely degraded photoactivity. In another word, the synergy effect between graphene and TNTs is important to the photoactivity.

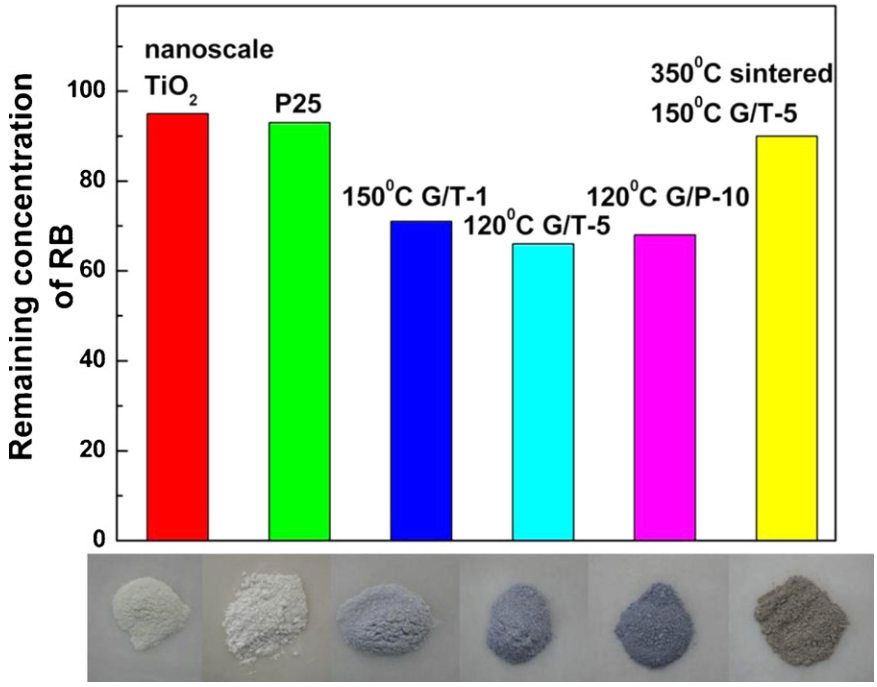

Fig. 9. Top: bar plot demonstrate the remaining Rhodamine-B in solution after reaching the adsorption equilibrium in the dark over nanoscale TiO_2, P25, 150 °C G/T-1, 120 °C G/T-5, 120 °C G/P-10 and 350 °C sintered 150 °C G/T-5 sintered material. Bottom: the digital images of these photocatalysts. The colors of photocatalysts become darker when the amount of graphene is increased.

4. Conclusion

A series of graphene/TNTs photocatalysts were fabricated by hydrothermal method at varied temperature. The unique tubular structures and large BET surface area of TNTs make it a promising visible-light driven photocatalyst after hybridizing with graphene. The UV–vis diffuse reflectance spectra, FTIR and XPS results confirm that the visible-light responses of these prepared photocatalysts are due to the sensitization of graphene rather than impurity level. The photocatalytic performances of them decrease in the order 120 °C samples > 150 °C samples > 180 °C samples, which is partially due to the decreased BET surface areas with increased hydrothermal temperatures. Moreover, the photocatalysts with proper amount of graphene (such as 5 wt%) combine the merits of graphene (sensitization effect and excellent carrier mobility) and TNTs (tubular structures and large BET surface area) well.

Acknowledgements

This work was supported by the National Natural Science Foundation of China (51076094, 50876062). The authors thank Instrumental Analysis Center of SJTU for FTIR measurement. The authors would like to thank Dr. Wei Chen for useful discussion and UV–vis diffuse reflectance spectroscopy measurement.

Appendix A. Supplementary data

Supplementary data associated with this article can be found, in the online version, at doi:10.1016/j.jhazmat.2011.10.012.

References

[1] K.S. Novoselov, A.K. Geim, S.V. Morozov, D. Jiang, Y. Zhang, S.V. Dubonos, I.V. Grigorieva, A.A. Firsov, Electric field effect in atomically thin carbon films, Science 306 (2004) 666–669.
[2] C. Lee, X. Wei, J.W. Kysar, J. Hone, Measurement of the elastic properties and intrinsic strength of monolayer graphene, Science 321 (2008) 385–388.
[3] B. Tang, G.X. Hu, H.Y. Gao, Raman spectroscopic characterization of graphene, Appl. Spectrosc. Rev. 45 (2010) 369–407.
[4] S.M. Peak, E.J. Yoo, I. Honma, Enhanced cyclic performance and lithium storage capacity of SnO_2/graphene nanoporous electrodes with three-dimensionally delaminated flexible structure, Nano Lett. 9 (2009) 72–75.
[5] B. Seger, P.V. Kamat, Electrocatalytically active graphene–platinum nanocomposites. Role of 2-D carbon support in PEM fuel cells, J. Phys. Chem. C 113 (2009) 7990–7995.
[6] K. Maeda, K. Teramura, D. Lu, T. Takata, N. Saito, Photocatalyst releasing hydrogen from water, Nature 440 (2006) 295.
[7] M. Fujihira, Y. Satoh, T. Osa, Heterogeneous photocatalytic oxidation of aromatic compounds on TiO_2, Nature 293 (1981) 206–208.
[8] D.V. Bavykin, A.A. Lapkin, P.K. Plucinski, Reversible storage of molecular hydrogen by sorption into multilayered TiO_2 nanotubes, J. Phys. Chem. B. 109 (2005) 19422–19427.
[9] S. Uchida, R. Chiba, M. Tomiha, N. Masaki, Application of titania nanotubes to a dye-sensitized solar cell, Electrochemistry 70 (2002) 418–420.
[10] R. Asahi, T. Morikawa, T. Ohwaki, K. Aoki, Y. Taga, Visible-light photocatalysis in nitrogen-doped titanium oxides, Science 293 (2001) 269–271.
[11] S. Khan, M. Al-Shahry, W.B. Ingler, Efficient photochemical water splitting by a chemically modified n-TiO_2, Science 297 (2002) 2243–2245.
[12] S. Sakthivel, H. Kisch, Daylight photocatalysis by carbon-modified titanium dioxide, Angew. Chem. Int. Ed. 42 (2003) 4908–4911.
[13] C. Wang, D.W. Bahnemann, J.K. Dohrmann, A novel preparation of iron-doped TiO_2 nanoparticles with enhanced photocatalytic activity, Chem. Commun. 16 (2000) 1539–1540.
[14] S. Livraghi, M.C. Paganini, E. Giamello, A. Selloni, C.D. Valentin, G. Pacchioni, Origin of photoactivity of nitrogen-doped titanium dioxide under visible light, J. Am. Chem. Soc. 128 (2006) 15666–15671.
[15] C.D. Valentin, G. Pacchioni, A. Selloni, Theory of carbon doping of titanium dioxide, Chem. Mater. 17 (2005) 6656–6665.
[16] Z.Y. Wang, C. Chen, F.Q. Wu, B. Zou, M. Zhao, J.X. Wang, C.H. Feng, Photodegradation of rhodamine B under visible light by bimetal codoped TiO_2 nanocrystals, J. Hazard. Mater. 164 (2009) 615–620.
[17] Y.P. Peng, S.L. Lo, H.H. Ou, Microwave-assisted hydrothermal synthesis of N-doped titanate nanotubes for visible-light-responsive photocatalysis, J. Hazard. Mater. 183 (2010) 754–758.
[18] V. Subramanian, E. Wolf, P.V. Kamat, Catalysis with TiO_2/gold nanocomposites. Effect of metal particle size on the fermi level equilibration, J. Am. Chem. Soc. 126 (2004) 4943–4950.
[19] E. Kowalska, H. Remita, J.C. Colbeau, J. Hupka, J. Belloni, Modification of titanium dioxide with platinum ions and clusters: application in photocatalysis, J. Phys. Chem. C 112 (2008) 1124–1131.
[20] X.Y. Zhang, H.P. Li, X.L. Cui, Y.H. Lin, Graphene/TiO_2 nanocomposites: synthesis, characterization and application in hydrogen evolution from water photocatalytic splitting, J. Mater. Chem. 20 (2010) 2801–2806.
[21] H. Zhang, X.J. Lv, Y.M. Li, Y. Wang, J.H. Li, P25–graphene composite as a high performance photocatalyst, ACS Nano 4 (2010) 380–386.
[22] W.S. Hummers, R.E. Offeman, Preparation of graphitic oxide, J. Am. Chem. Soc. 80 (1958) 1339.
[23] Y. Wang, Y.M. Li, L.H. Tang, J. Lu, J.H. Li, Application of graphene-modified electrode for selective detection of dopamine, Electrochem. Commun. 11 (2009) 889–892.
[24] D.H. Wang, D.W. Choi, J. Li, Self-assembled TiO_2–graphene hybrid nanostructures for enhanced Li-ion insertion, ACS Nano 3 (2009) 907–914.
[25] J.C. Zhao, T.X. Wu, K.Q. Wu, K. Oikawa, Photoassisted degradation of dye pollutants. 3. Degradation of the cationic dye Rhodamine-B in aqueous anionic surfactant/TiO_2 dispersions under visible light irradiation: evidence for the need of substrate adsorption on TiO_2 particles, Environ. Sci. Technol. 32 (1998) 2394–2400.
[26] W.L. Zhang, Y. Li, C. Wang, P.F. Wang, Kinetics of heterogeneous photocatalytic degradation of rhodamine B by TiO_2-coated activated carbon: role of TiO_2 content and light intensity, Desalination 266 (2011) 40–45.
[27] Y.L. Pang, S. Bhatia, A.Z. Abdullah, Process behavior of TiO_2 nanotube-enhanced sonocatalytic degradation of Rhodamine B in aqueous solution, Sep. Purif. Technol. 77 (2011) 331–338.
[28] C. Chen, M.C. Long, H. Zeng, W.M. Cai, Preparation, characterization and visible-light activity of carbon modified TiO_2 with two kinds of carbonaceous species, J. Mol. Catal. A: Chem. 314 (2009) 35–41.
[29] L.W. Zhang, H.B. Fu, Y.F. Zhu, Efficient TiO_2 photocatalysts from surface hybridization of TiO_2 particles with graphite-like carbon, Adv. Funct. Mater. 18 (2008) 2180–2189.
[30] Q. Chen, W.Z. Zhou, G.H. Du, Trititanate nanotubes made via a single alkali treatment, Adv. Mater. 14 (2002) 1208–1211.
[31] D. Wu, Y.F. Chen, J. Liu, X.N. Zhao, Preparation and structure analysis of titanium oxide nanotubes, Appl. Phys. Lett. 87 (2005) 112501–112503.
[32] A.B. Bourlinos, D. Gournis, D. Petridis, T. Szabo, A. Szeri, I. Dekany, Graphite oxide: chemical reduction to graphite and surface modification with primary aliphatic amines and amino acids, Langmuir 19 (2003) 6050–6055.
[33] B. Neumann, P. Bogdanoff, H. Tributsch, S. Sakthivel, H. Kisch, Electrochemical mass spectroscopic and surface photovoltage studies of catalytic water photooxidation by undoped and carbon-doped titania, J. Phys. Chem. B 109 (2005) 16579–16586.
[34] Q. Xiao, J. Zhang, C. Xiao, Z. Si, X. Tan, Solar photocatalytic degradation of methylene blue in carbon-doped TiO_2 nanoparticles suspension, Solar Energy 82 (2008) 706–713.
[35] J. Pouilleau, D. Devilliers, H.P. Groult, Surface of a titanium-based ceramic electrode material by X-ray photoelectron spectroscopy, J. Marcus Mater. Sci. 32 (1997) 5645–5651.
[36] G. Williams, B. Seger, P.V. Kamat, TiO_2–graphene nanocomposites UV-assisted photocatalytic reduction of graphene oxide, ACS Nano 2 (2008) 1487–1491.
[37] A. Iwabuchi, C. Choo, K. Tanaka, Titania nanoparticles prepared with pulsed laser ablation of rutile single crystals in water, J. Phys. Chem. B 108 (2004) 10863–10871.
[38] C. Chen, W.M. Cai, M.C. Long, J.Y. Zhang, B.X. Zhou, Y.H. Wu, Template-free sol–gel preparation and characterization of free-standing visible light responsive C,N-modified porous monolithic TiO_2, J. Hazard. Mater. 178 (2010) 560–565.
[39] K.M. Kiran, Y. Zhou, Y.L. Yan, P.L. Kian, Multilayer hybrid films consisting of alternating graphene and titania nanosheets with ultrafast electron transfer and photoconversion properties, Adv. Funct. Mater. 19 (2009) 3638–3643.
[40] Y. Wang, X.H. Chen, Y.L. Zhong, Large area, continuous, few-layered graphene as anodes in organic photovoltaic devices, Appl. Phys. Lett. 95 (2009) 063303–063305.
[41] F.B. Su, X.S. Zhao, Y. Wang, J.H. Zeng, Synthesis of graphitic ordered macroporous carbon with a three-dimensional interconnected pore structure for electrochemical applications, J. Phys. Chem. B 109 (2005) 20200–20206.
[42] D. Ulrike, T.E. Madey, TiO_2 by XPS, Surf. Sci. Spectra 4 (1996) 227–231.
[43] F.B. Li, M.F. Hou, K.W. Cheah, W.C.H. Choy, Enhanced photocatalytic activity of Ce^{3+}–TiO_2 for 2-mercaptobenzothiazole degradation in aqueous suspension for odour control, Appl. Catal. A: Gen. 285 (2005) 181–189.
[44] P. Salvador, On the nature of photogenerated radical species active in the oxidative degradation of dissolved pollutants with TiO_2 aqueous suspensions: a revision in the light of the electronic structure of adsorbed water, J. Phys. Chem. C 111 (2007) 17038–17043.